Supplementary Materials for

Soft, wireless periocular wearable electronics for real-time detection of eye vergence in a virtual reality toward mobile eye therapies

Saswat Mishra[1*], Yun-Soung Kim[1*], Jittrapol Intarasirisawat[2], Young-Tae Kwon[1], Yongkuk Lee[3], Musa Mahmood[1], Hyo-Ryoung Lim[1], Robert Herbert[1], Ki Jun Yu[4], Chee Siang Ang[2], Woon-Hong Yeo[1,5,6]†

[1]George W. Woodruff School of Mechanical Engineering, Institute for Electronics and Nanotechnology, Georgia Institute of Technology, Atlanta, Georgia 30332, USA.

[2]School of Engineering and Digital Arts, Jennison Building, University of Kent, Canterbury, Kent, CT2 7NT, UK.

[3]Department of Biomedical Engineering, Wichita State University, Wichita, Kansas 67260, USA.

[4]School of Electrical and Electronic Engineering, Yonsei University, Seoul 03722, Republic of Korea.

[5]Wallace H. Coulter Department of Biomedical Engineering, Parker H. Petit Institute for Bioengineering and Biosciences, Georgia Institute of Technology and Emory University, Atlanta, Georgia 30332, USA.

[6]Center for Flexible and Wearable Electronics Advanced Research, Institute for Materials, Neural Engineering Center, Georgia Institute of Technology, Atlanta, Georgia 30332, USA.

*These authors contributed equally to this work.

†Corresponding author. Email: whyeo@gatech.edu (W.-H.Y.)

This PDF file includes:

Table S5. OV2 real-time classification of test subjects using the physical apparatus.
Table S6. OV2 real-time classification of test subjects using the physical apparatus.
Video S1. An example of a real-time vergence detection with a physical apparatus.
Video S2. An example of operation of a VR program – Brock string.
Video S3. An example of a real-time VR-based training apparatus.

Section S1. Conformal contact analysis for aerosol jet printed electrodes

For conformal contact to occur, the magnitude of adhesion energy must be larger than the sum of the bending and elastic energy. Equation (1) describes this condition.

$$0 < U_{bending} + U_{skin} + U_{adhesion} \tag{1}$$

Then, defining each of these energy terms. Bending energy is defined as:

$$U_{bending} = \frac{1}{\lambda_{rough}} \int_0^{\lambda_{rough}} \frac{EI_{electrode}(w'')^2}{2} dx = \frac{\pi^4 EI_{electrode} h^2}{\lambda_{rough}^4} \tag{2}$$

The bending stiffness, $EI_{electrode}$, is calculated via:

$$EI_{electrode} = \alpha EI_{PI/Ag} + (1-\alpha) EI_{silicone} \tag{3}$$

where α is the PI/Ag area fraction of the skin-like electrode. The bending stiffness is split into that for the silicone elastomer layer and the PI/Ag pattern:

$$EI_{silicone} = E_{silicone} {h_{silicone}}^3/12 \tag{4}$$

$$EI_{PI/Ag} = \sum_{i=1}^{N} E_i h_i \left[\left(b - \sum_{j=1}^{i} h_j \right)^2 + \left(b - \sum_{j=1}^{i} h_j \right) h_i + \frac{1}{3} h_i^2 \right] \tag{5}$$

$$b = \sum_{i=1}^{N} E_i h_i \left(\sum_{j=1}^{i} h_j - \frac{1}{2} h_i \right) / \sum_{i=1}^{N} E_i h_i \tag{6}$$

The skin surface is modeled with a sine wave as:

$$w(x) = \frac{h}{2} \left(1 + \cos \frac{2\pi x}{\lambda_{rough}} \right) \tag{7}$$

While the displacement of the electrode is defined as:

$$u_z(x) = y - w = \frac{h_{rough} - h}{2} \left(1 + \cos \frac{2\pi x}{\lambda_{rough}} \right) \tag{8}$$

We assume the following dimensions to represent the properties of human skin:

$$h_{rough} = 55\ \mu m \qquad \lambda_{rough} = 140\ \mu m \qquad E_{skin} = 130\ kPa$$

where h_{rough} is roughness amplitude, λ_{rough} is wavelength, and E_{skin} is the modulus of skin.

The elastic energy of the skin, due to normal stress, is defined as:

$$\sigma_z = \frac{\pi E_{skin} (h_{rough} - h)}{2\lambda_{rough}} \cos \frac{2\pi x}{\lambda_{rough}} \tag{9}$$

$$U_{skin} = \frac{1}{\lambda_{rough}} \int_0^{\lambda_{rough}} \frac{\sigma_z u_z}{2} dx = \frac{\pi E_{skin} (h_{rough} - h)^2}{16\lambda_{rough}} \tag{10}$$

The interfacial adhesion energy is calculated as:

$$U_{adhesion} = -\gamma \int_0^{\lambda_{rough}} \sqrt{1 + (w')^2} dx \approx -\gamma \left(1 + \frac{\pi^2 h^2}{4\lambda_{rough}^2} \right) \text{ for the case } \lambda_{rough} \sim 7 h_{rough} \tag{11}$$

The work of adhesion value is dominated by the elastomer, and the electrode's total value is:

$$\gamma = (1-\alpha) \gamma_{silicone/skin} \tag{12}$$

Minimizing the total energy to express maximum deflection of the electrode results in terms of h:

$$h = \frac{E_{skin} h_{rough}}{\frac{16\pi^3 EI_{electrode}}{\lambda_{rough}^3} + E_{skin}} \tag{13}$$

Then, substituting into equation (1):

$$U_{bending} + U_{skin} + U_{adhesion} = -0.150\, J$$

Thus, conformal contact occurs between the electrode and skin.

Parameters used in this calculation include:

$E_{silicone}$	7.85 kPa
$\gamma_{silicone/skin}$	0.89
E_{PI}	2.5 GPa
E_{Ag}	69 GPa
$h_{silicone}$	65 μm
h_{PI}	1 μm
h_{Ag}	1 μm
α	33.47%

Section S2. Methods for cross-validation

After the data is recorded it is stored into a .mat file for further processing. The data is stored in a double structure which is then separated in MATLAB cell arrays. The cell arrays are inserted into a Butterworth bandpass filter between, 0.01 Hz and 10 Hz. A zero-phase filter is implemented after data is recorded, while the real-time data is parsed in to 500 ms windows that are filtered after 5 s of data is recorded. The filtered data is separated into 10 features that are inserted into the classifier for cross-validation. Numerous classifiers were compared in classification learner application prior to establishing the ensemble subspace discriminant as the best classifier by utilizing five-fold cross-validation with each classifier. MATLAB's cross-validation algorithm applies randomization of the training and testing data by splitting the data into five folds and six groups. Five out of the six groups are randomly indicated as training and the last group is randomly indicated as the testing group. The groups are divided into n groups equal to the number of classes. The output class is presented in a confusion matrix at the end of recording as well as real-time on the graphical user interface. This approach was utilized with all 14 test subjects with a minimum of at least three attempts from each subject towards training and testing.

Section S3. Fabrication and assembly process

Fabrication process of flexible devices including conventional microfabrication techniques, double transfer printing process, direct writing on soft material with additive manufacturing, and chip mounting.

a) Preparation of a carrier wafer

1. Clean a silicon wafer with acetone, IPA, and DI water.
2. Dehydrate on a hot plate at 110 °C for 3 min.
3. Apply O_2 plasma at 50 W for 60 sec.
4. Spincoat PMMA A7 at 4000 rpm for 30 sec.
5. Bake on a hot plate at 180 °C for 2 min 30 sec.
6. Spincoat PI (PI) at 4000 rpm for 1 min.
7. Pre-bake on a hot plate at 150 °C for 5 min.
8. Hard bake on a hot plate at 250 °C for 55 min.

b) Material deposition and photolithography

1. Deposit 1 μm -thick copper (Cu) using sputtering systems.
2. Spincoat photoresist (AZ 4620) at 2000 rpm for 30 sec.
3. Bake on a hot plate at 110 °C for 5 min.
4. Align with a photomask and expose UV light, exposure dose of 320 mJ/cm^2.
5. Develop patterns with a developer (AZ 400K , 1:3 dilution).
6. Etch Cu using copper etchant.
7. Remove photoresist using acetone.
8. Dehydrate on a hot plate at 110 °C for 3 min.
9. Apply O_2 plasma at 50 W for 30 sec.
10. Spincoat PI at 900 rpm for 1min.
11. Bake on a hot plate at 150 °C for 5 min and 200 °C for 15 min.
12. Spincoat second PI at 900 rpm for 1 min.
13. Bake on a hot plate at 150 °C for 5 min and 200 °C for 45 min.
14. Apply O_2 plasma at 50 W for 30 sec.
15. Spincoat photoresist (AZ 4620) at 2000 rpm for 30 sec.
16. Bake on a hot plate at 110 °C for 5 min.
17. Align with a photomask and expose UV light, exposure dose of 320 mJ/cm^2.
18. Develop patterns with a developer (AZ 400K , 1:3 dilution).

19. Etch PI using reactive ion etcher (RIE) at 150 W, 150 mTorr, and 20 sccm O_2 for 18 min.
20. Remove photoresist using acetone.
21. Dehydrate on a hot plate at 110 °C for 3 min.
22. Apply O_2 plasma at 50 W for 30 sec.
23. Deposit 2 μm-thick Cu using sputtering systems.
24. Spincoat photoresist (AZ 4620) at 2000 rpm for 30 sec.
25. Bake on a hot plate at 110 °C for 5 min.
26. Align with a photomask and expose UV light, exposure dose of 320 mJ/cm^2.
27. Develop patterns with a developer (AZ 400K , 1:3 dilution).
28. Etch Cu using copper etchant.
29. Remove photoresist using acetone.
30. Dehydrate on a hot plate at 110 °C for 3 min.
31. Apply O_2 plasma at 50 W for 30 sec.
32. Spincoat PI at 4000 rpm for 1min.
33. Bake on a hot plate at 150 °C for 5 min and 200 °C for 45 min.
34. Apply O_2 plasma at 50 W for 30 sec.
35. Spincoat photoresist (AZ 4620) at 2000 rpm for 30 sec.
36. Bake on a hot plate at 110 °C for 5 min.
37. Align with a photomask and expose UV light, exposure dose of 320 mJ/cm^2.
38. Develop patterns with a developer (AZ 400K , 1:3 dilution).
39. Etch PI using reactive ion etcher (RIE) at 150 W, 150 mTorr, and 20 sccm O_2 for 30 min.
40. Remove photoresist using acetone.

c) Preparation of a thin elastomeric membrane

1. Prepare 4 g of 1:1 Ecoflex00-30 and 6 g of 1:1 Ecoflex Gel and mix them together.
2. Spincoat the mixture at 200 rpm for 30 sec on 5 inch plastic petri dish.
3. Cure at room temperature.

d) Pick up and transfer printing of intraoral electronic device

1. Immerse fabricated intraoral electronic circuit on wafer in acetone overnight.
2. Pick up the intraoral electronic circuit using water-soluble tape.
3. Transfer onto thin elastomeric membrane.

4. Dissolve the water-soluble tape by gently applying water.

e) Mount electronic chips

1. Screen print low temperature solder paste (alloy of Sn/Bi/Ag (42%/57.6%/0.4%), Chip Quik Inc.) with alignment on the intraoral electronic circuit.
2. After mounting all necessary chips on proper contact pads, apply heat according to recommended reflow profile.
3. Apply soldering Flux if necessary.
4. Attach a 1x1x1 mm^3 neodynium magnet to sensor pads for complete circuit.

f) Fabrication of skin-like electrode with Aerosol Jet Printing

1. Prepare a glass slide by cleaning with acetone and IPA.
2. Spin coat PMMA A7 thickness of 700 nm at 4000 RPM for 30 seconds.
3. Bake the PMMA for 2 min 30 sec..
4. Spin coat a layer of PI 2545, thickness of 1 µm at 5000 RPM for 1 minute.
5. Bake the PI-2545 for 60 minutes at 250°C on a hotplate.
6. Surface treat the sample with air plasma for 30 seconds.
7. Load sample on aerosol jet print (AJP) platen and set temperature to 70 °C.
8. Turn on the sheath flow rate at 30 SCCM.
9. Turn on the atomizer flow rate at 20 SCCM.
10. Turn on the atomizer current at 0.6 Amps.
11. Deposit silver by running the program.
12. Sinter the nanoparticles at 200 °C for 1 hour.
13. Load sample on AJP platen and set temperature to 70 °C.
14. Turn on the sheath flow rate at 30 SCCM.
15. Turn on the atomizer flow rate at 20 SCCM.
16. Turn on the atomizer current at 0.6 Amps.
17. Align silver layer with next layer using fiducial markers.
18. Deposit diluted SC1813 by running the program.

19. Bake for 5 minutes at 110°C.

20. Etch PI using reactive ion etcher (RIE) at 250 W, 150 mTorr, and 20 sccm O_2 for 20 min.

21. Remove photoresist with acetone.

g) Pick up and transfer printing of AJP skin-like electrode

1. Clean a glass slide with acetone and IPA and dehydrate at 100 °C.
2. Laminate a film of polyvinyl alcohol (PVA) onto the glass slide with scotch tape.
3. Prepare 2.5 g of Ecoflex gel mixture 1:1 and spin coat it at 2000 RPM for 1 min.
4. Let Ecoflex gel cure at room temperature for 2 hours.
5. Take the skin-like electrode sample and place into a bath of acetone.
6. Heat up the acetone bath at 60 °C for 1 hour.
7. Transfer the sample with a PVA based water-soluble tape.
8. Place the transferred samples and the tape onto the Ecoflex gel substrate.
9. Hydrate the tape to dissolve.
10. Attach anisotropic conductive film (ACF) wires to the skin-like electrode on the pad side.
11. Attach a 1x1x1 mm^3 magnet to the wire with silver paint.

Section S4. Vergence physical apparatus and VR system

After device and sensor fabrication, it is ready to be used on a test subject for testing with physical apparatus or virtual reality apparatus.

a) Physical Apparatus

1. Place electrodes in desired position, conventional, OV1, or OV2.
2. Place device on shirt if using conventional radio or place flexible device on back of the neck.
3. Setup physical apparatus in a room with 500x500cm of space.
4. Assist the participant by placing their head on the ocular headstand for stability during testing.
5. Instruct the participant to follow the commands from the MATLAB program.
6. After 70 seconds, record the data by selecting each trial and position on the apparatus individually.
7. After five trials are recorded, press the cross-validation button to assess your dataset.

b) Virtual Apparatus

1. Place electrodes in desired position, conventional, OV1, or OV2.
2. Place device on shirt if using conventional radio or place flexible device on back of the neck.
3. Initiate the correct application on the Samsung S6 and then place the Samsung S6 in gear VR.
4. Assist the participant by placing the Samsung S6 and Samsung gear VR on the head.
5. After tightening straps, instruct the user to initiate the program at the same time as the MATLAB program.
6. After 70 seconds, record the data by selecting each trial and position on the apparatus individually.
7. After five trials are recorded, press the cross-validation button to assess your dataset.

Supplementary Figures

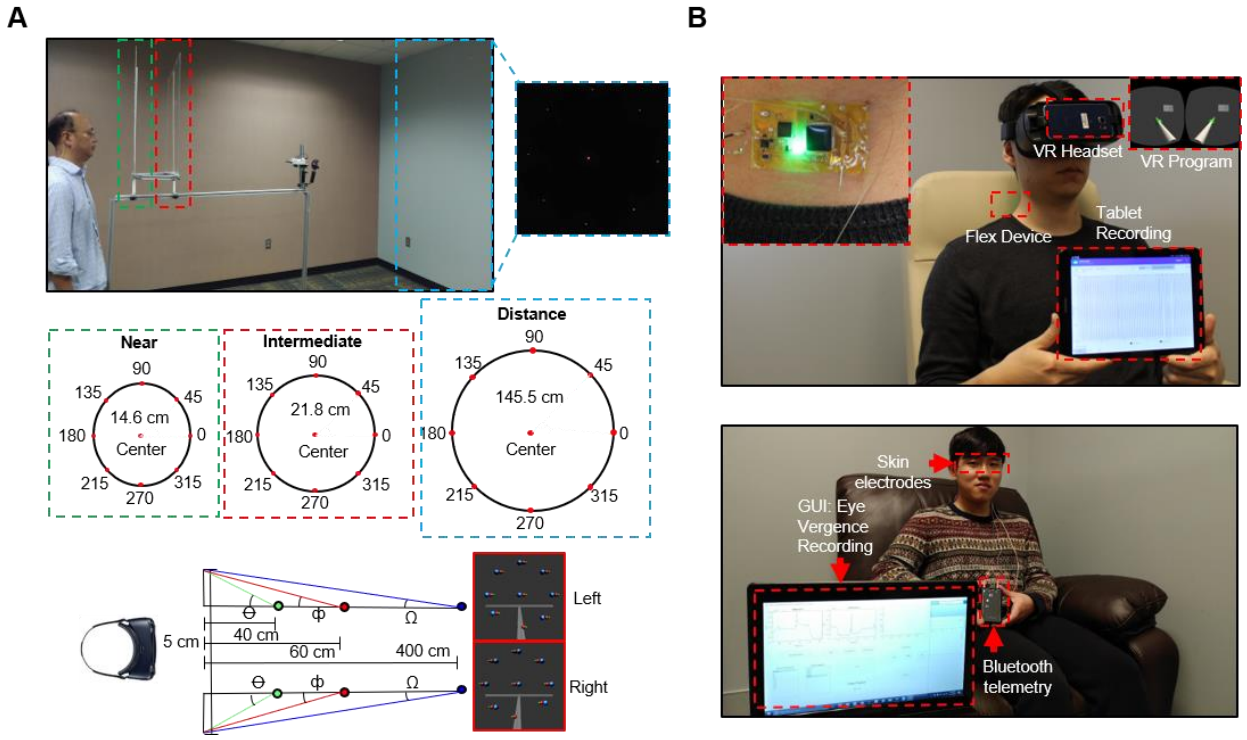

Figure S1. Apparatus for testing eye vergence motions. (A) The setup of the physical apparatus (top). Dimensions of the apparatus for the physical consists of positions that approximate to 1º, 2º, and 3º of motion (middle). The VR images are offset for each eye to simulate binocular vision in the real world (bottom). (B) Data collection methods for periocular wearable electronics and BioRadio. Flexible device data collection with an Android device (top) and conventional data acquisition with rigid Bluetooth device and MATLAB interface (bottom).

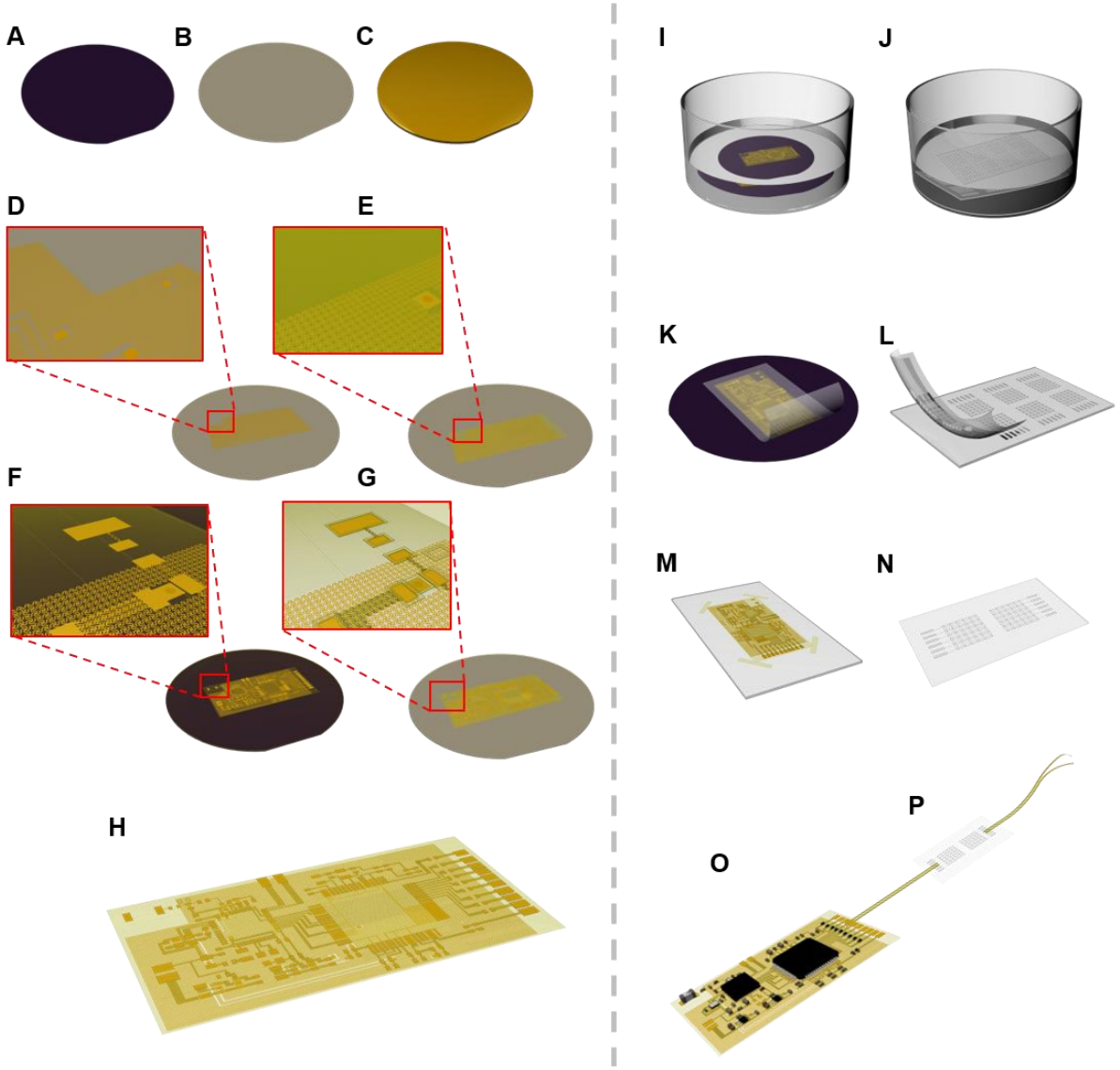

Figure S2. Fabrication and assembly processes for the flexible device and the skin-like electrodes. (A) Flexible device fabrication is conducted using a clean silicon wafer on which to build (B) a layer of PMMA and PI. (C) Sputter copper and then (D) etch the copper with APS-100. (E) Spin cast two layers of PI and etch the holes. (F) Deposit copper to fill in holes and create top interconnect layer. (G) Spin cast PI and etch away the top layer. (H) Finished design is ready to transfer after removing any copper oxides using stainless steel flux. (I) Flexible device is submerged in a bath of acetone at 60 ºC overnight (J) while the skin-like electrode is processed in the acetone bath for 1 hour. (K) Use the water-soluble tape to transfer the device off the silicon wafer and (L) skin-like electrode off the glass slide. (M) Prepare the Ecoflex gel and Ecoflex 30 mixture for the device and transfer simultaneously prepare the (N) Ecoflex gel sample on PVA for the skin-like electrodes. (O) Solder the IC chips onto the thin film flexible board and (P) attach ACF wires to the skin-like electrodes then configure the device and the skin-like electrodes together.

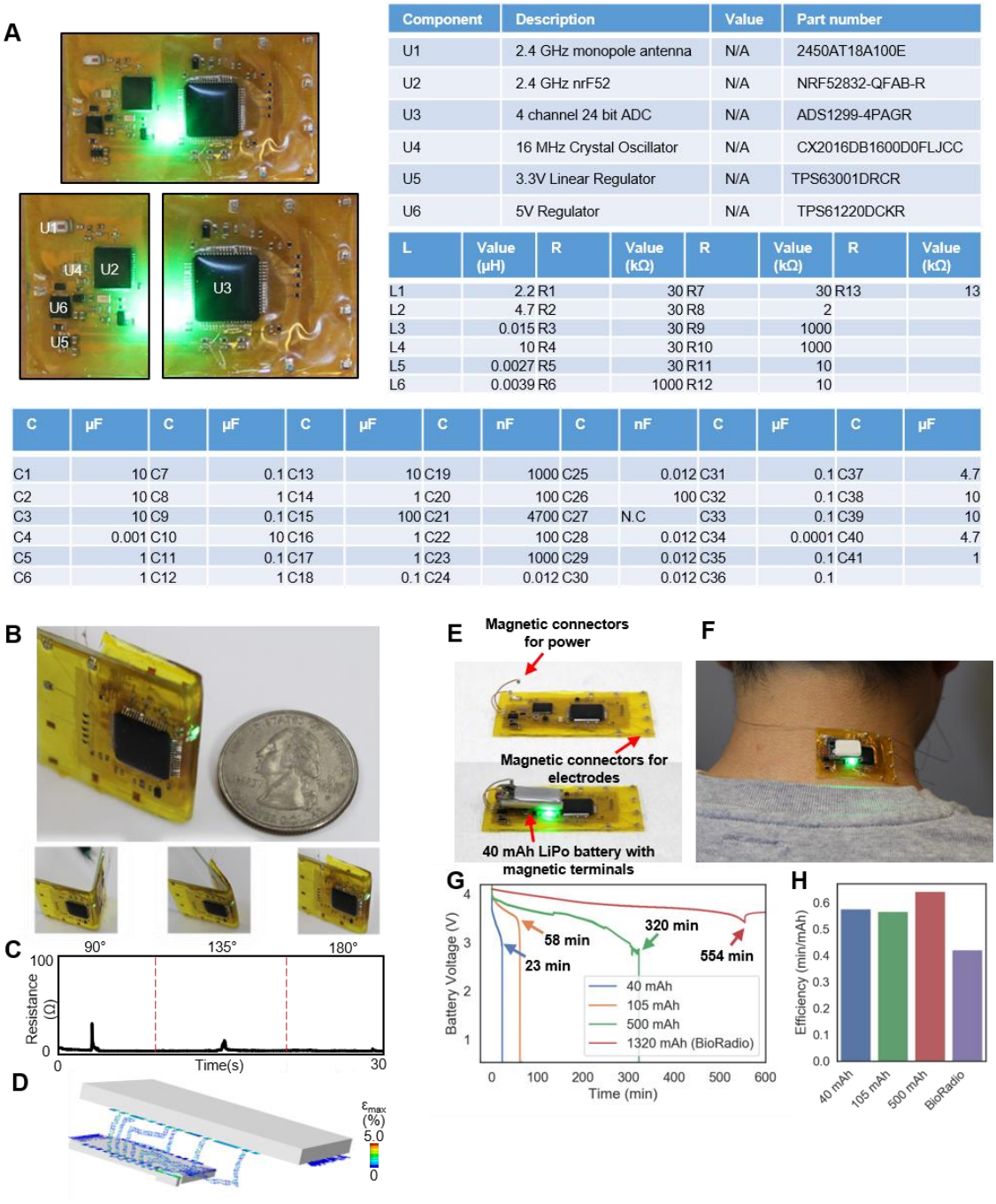

Component	Description	Value	Part number
U1	2.4 GHz monopole antenna	N/A	2450AT18A100E
U2	2.4 GHz nrF52	N/A	NRF52832-QFAB-R
U3	4 channel 24 bit ADC	N/A	ADS1299-4PAGR
U4	16 MHz Crystal Oscillator	N/A	CX2016DB1600D0FLJCC
U5	3.3V Linear Regulator	N/A	TPS63001DRCR
U6	5V Regulator	N/A	TPS61220DCKR

L	Value (μH)	R	Value (kΩ)	R	Value (kΩ)	R	Value (kΩ)
L1	2.2	R1	30	R7	30	R13	13
L2	4.7	R2	30	R8	2		
L3	0.015	R3	30	R9	1000		
L4	10	R4	30	R10	1000		
L5	0.0027	R5	30	R11	10		
L6	0.0039	R6	1000	R12	10		

C	μF	C	μF	C	μF	C	nF	C	nF	C	μF	C	μF
C1	10	C7	0.1	C13	10	C19	1000	C25	0.012	C31	0.1	C37	4.7
C2	10	C8	1	C14	1	C20	100	C26	100	C32	0.1	C38	10
C3	10	C9	0.1	C15	100	C21	4700	C27	N.C	C33	0.1	C39	10
C4	0.001	C10	10	C16	1	C22	100	C28	0.012	C34	0.0001	C40	4.7
C5	1	C11	0.1	C17	1	C23	1000	C29	0.012	C35	0.1	C41	1
C6	1	C12	1	C18	0.1	C24	0.012	C30	0.012	C36	0.1		

Figure S3. Circuit components, bending, and powering of the flexible device. (A) The photograph of the flexible device details the locations for the chip components and the tables list the parts used in the design. (B) Device is compared to the American quarter showing the size of the device (top). (C) Successive bending of the device from 90°- 180° shows minor fluctuations in resistance and continuous operation of the device. (D) FEA simulation of device bending. (E) Photographs show the integration of the small lithium-ion polymer battery with miniaturized magnetic terminals. Two wires with respective magnetic polarities enables the easy battery integration. As pointed by the arrow on the right, the same magnetic connectors are allocated for EOG signals. (F) Operation of the device on the back of the user's neck. ACF wires with magnetic terminals allow for reversible wire attachment. (G) Battery voltage measurements of periocular wearable electronics and BioRadio. Arrows indicate data points when Bluetooth is disconnected. (H) Efficiency for periocular wearable electronics with various battery capacities and BioRadio (1320 mAh) calculated by dividing the time of operation by battery capacity.

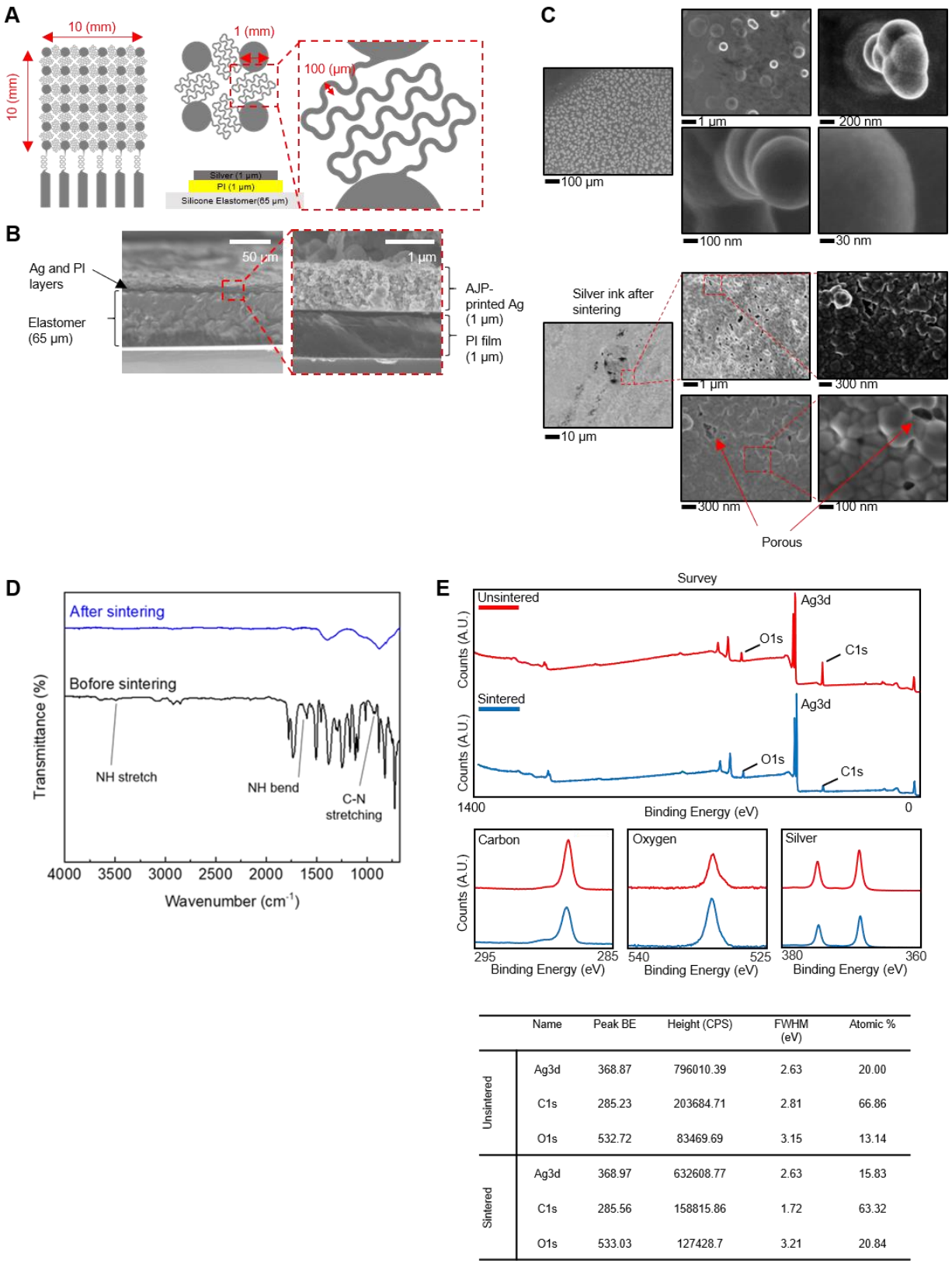

	Name	Peak BE	Height (CPS)	FWHM (eV)	Atomic %
Unsintered	Ag3d	368.87	796010.39	2.63	20.00
	C1s	285.23	203684.71	2.81	66.86
	O1s	532.72	83469.69	3.15	13.14
Sintered	Ag3d	368.97	632608.77	2.63	15.83
	C1s	285.56	158815.86	1.72	63.32
	O1s	533.03	127428.7	3.21	20.84

Figure S4. Design and characterization of the AgNP electrodes. (A) Skin-like electrode's dimensions are 1x1 cm2 and is consisted with an array of 1 mm diameter circles interconnected with fractal-shaped traces. The circular feature increases the overall contact area while the fractal-shaped interconnection enables stretching. The radius of each curve is 100 μm with a trace width ranging from 20 μm – 60 μm depending on the type process used. (B) Cross-sectional SEM images

revealing the morphology and thickness of the layers comprising the skin-like electrode. The close-up image on the right shows the thin PI/Ag bilayer structure. (C) SEM images of AgNP ink after deposition and degassed (top) and after sintering (bottom). (D) FTIR transmittance spectra of aerosol jet printed pattern before and after sintering. Peaks present in the 'before sintering' sample are from (i) oleylamine, (ii) solvent (aromatic) in Ag ink, and (iii) PI. 'After sintering' curve contains only the general PI peaks and metallic Ag. (E) XPS characterization of AgNPs before sintering and after sintering. A survey of the AgNP ink solution indicates carbon, oxygen, and silver. The concentrations of oxygen and carbon change after sintering the sample.

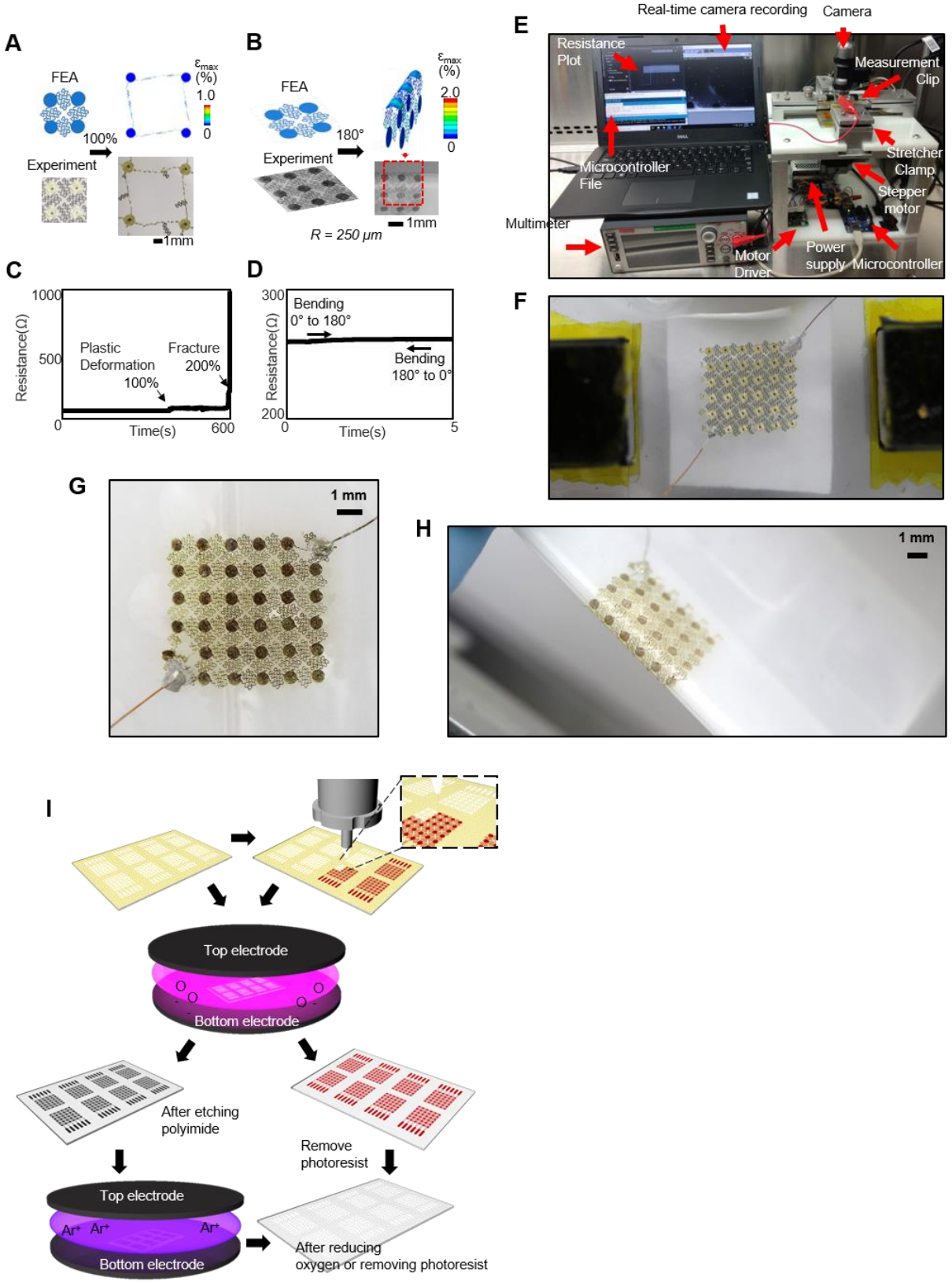

Figure S5. Stretching/bending properties of the skin-like electrodes fabricated by AJP. (A) FEA simulation of open mesh sensor stretching and bending. Electrode is stretched up to 100% before there is a change in resistance. (B) The electrode is then bent 180° at a bending radius of 250 μm. (C) The resistance of the electrode increases as the biaxial stretcher passes 100% stretchability

up to 200% where the sensor fractures. (D) Loading and unloading of the sensor shows no resistance change therefore the device continues to function flawlessly. (E) The computer vision for monitoring the skin-like electrode stretching with resistance measurements from the digital multimeter. (F) The contact for the resistance measurements is made possible with copper wire and silver paste from end to end contact. (G) Skin-like electrode setup for bending test with 250 μm bending radius (H) Electrode bent by 180º. (I) Skin-like electrode direct writing process and post processing using reactive ion etching and reduction of silver nanoparticles. After atomization and deposition, a full electrode array is ready to be processed by dry etching. There are two options for dry etching, first option is to etch the PI after printing and second option is to deposit photoresist onto the silver patterns by alignment. A close up shows the deposition location and the beam diameter of 5 μm. After depositing all electrodes on the substrate, the sample can be treated in oxygen plasma to etch the PI. After etching, oxygen has impinged the silver and needs to be reduced or the photoresist stays intact, and the silver is protected while the PI is etched away. The final reduction step is conducted in a RIE with argon gas which removes most of the oxygen. The final electrode array comes out of the RIE bright white after removing photoresist or reducing.

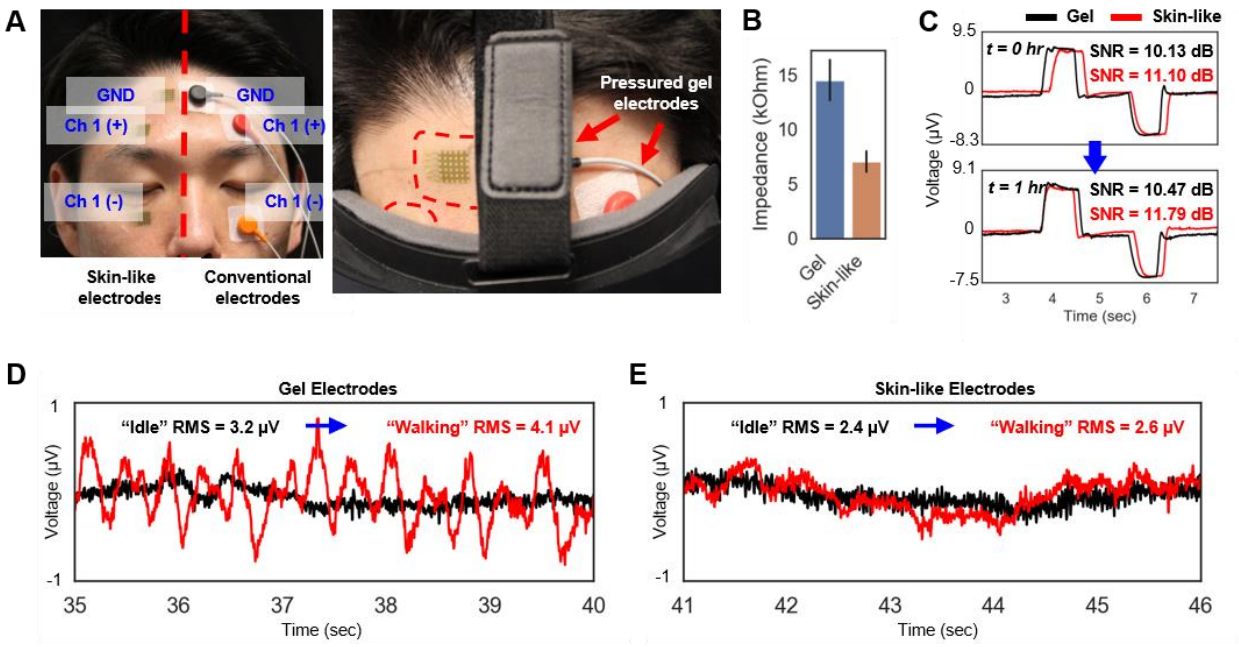

Figure S6. Comparison between Ag/AgCl gel electrodes and aerosol get printed skin-like electrodes. (A) Electrode placement for the simultaneous comparison of the two types of electrodes. Each pair of electrodes is placed above and below each eye for detection of vertical eye movements along with respective ground electrodes. (B) Photograph reveals the snug fitting of the nanomembrane electrodes (highlighted with dashed lines) whereas the gel electrodes and wires can be seen pressured by the VR headset, causing discomfort and incorrect fitting of the headset (red arrows). (C) Average skin-like electrode impedance values of the electrodes. (D) SNR analysis of EOG from 10 trials of the vertical eye movement protocol at the start and finish of the 1-hour session. The plots show raw EOG signals from one trial each from start and finish of the session. (E) RMS analysis of the EOG signals recorded while sitting down and walking on a treadmill at 3.2 mph. The subject stared at a fixed marker during the 1-minute session without blinking. The plots show the 5-second snapshots of the raw EOG signals during walking.

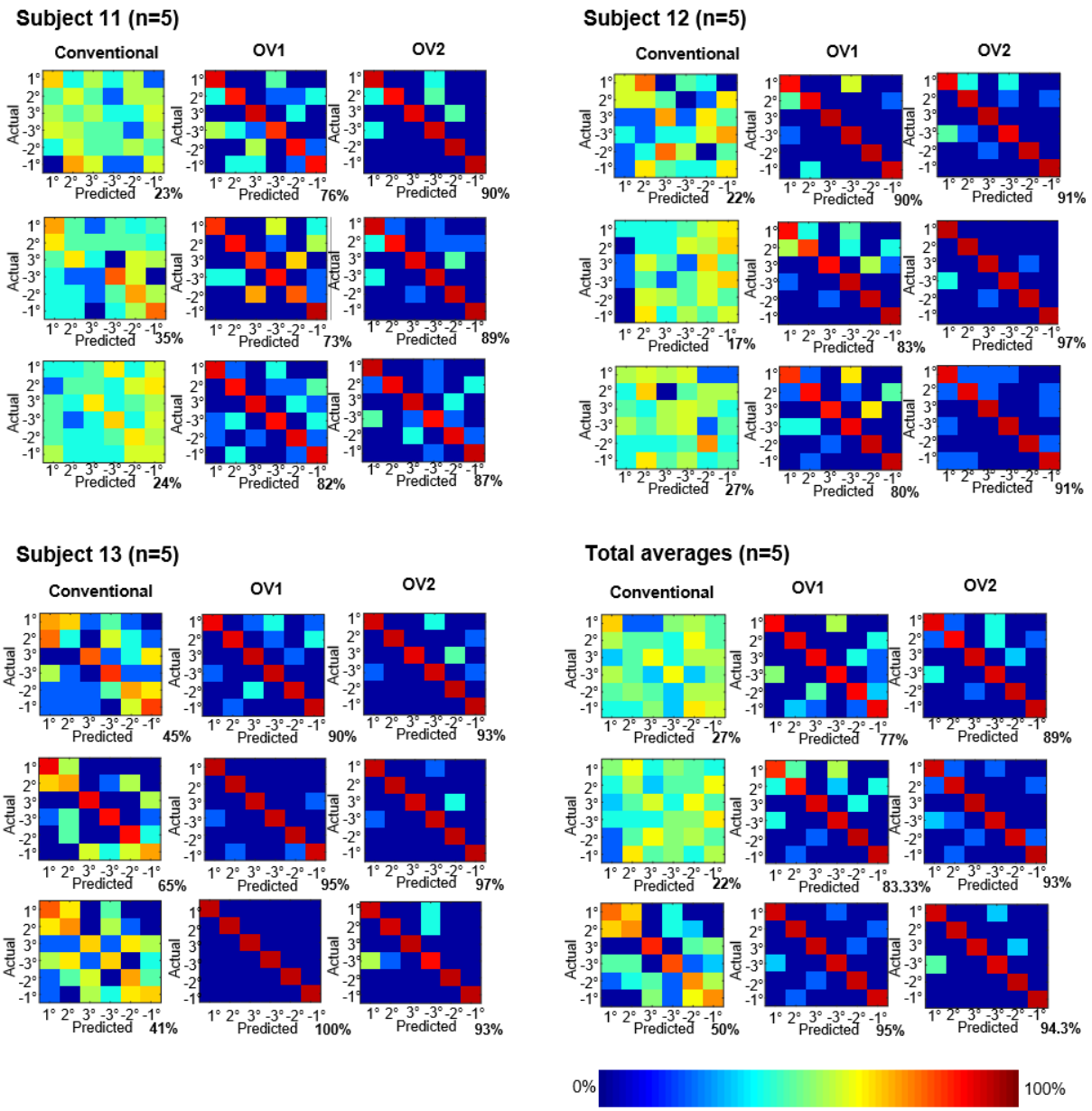

Figure S7. Electrode assessment for subject 11-13. Confusion matrices for subject 11 through 13 using the virtual reality training platform.

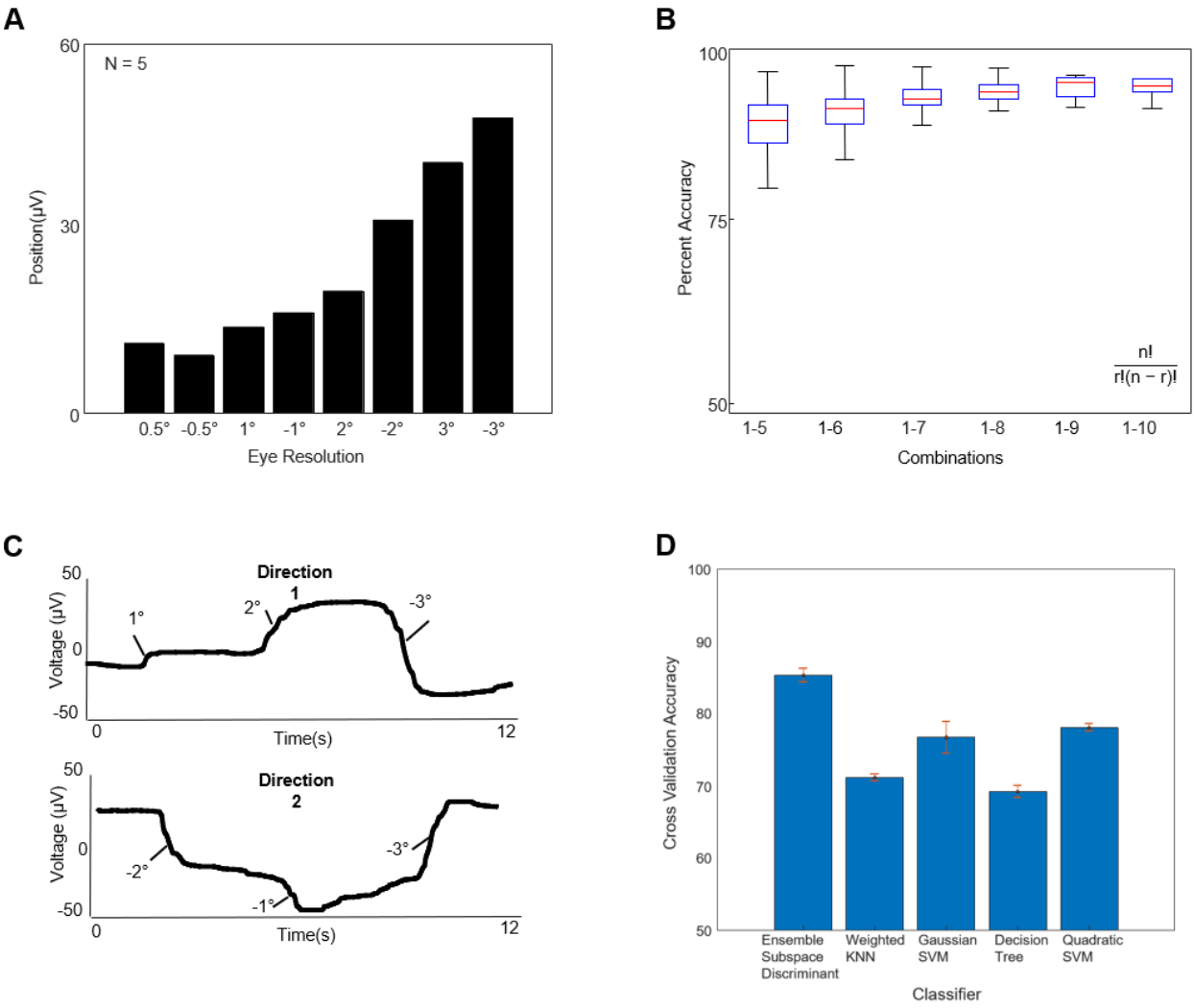

Figure S8. Performances of the periocular wearable electronics. (A) Eye resolution of subject 12 was observed to be as low as 15 μV for 0.5° of eye vergence in the VR headset. (B) Percent of accuracy with permutations of features from all three channels for position and velocity. (C) The procedure for recording and training eye vergence involves following a linear procedure to extract all eye motions equal number of times. Direction 1 (top) and direction 2 (bottom) are repeated four times. (D) Cross-validation accuracy of five-fold validation amongst five high ranking classifier accuracies from classification learner application. Subject 12 demonstrates highest average accuracy of 85% with standard deviation of 2%.

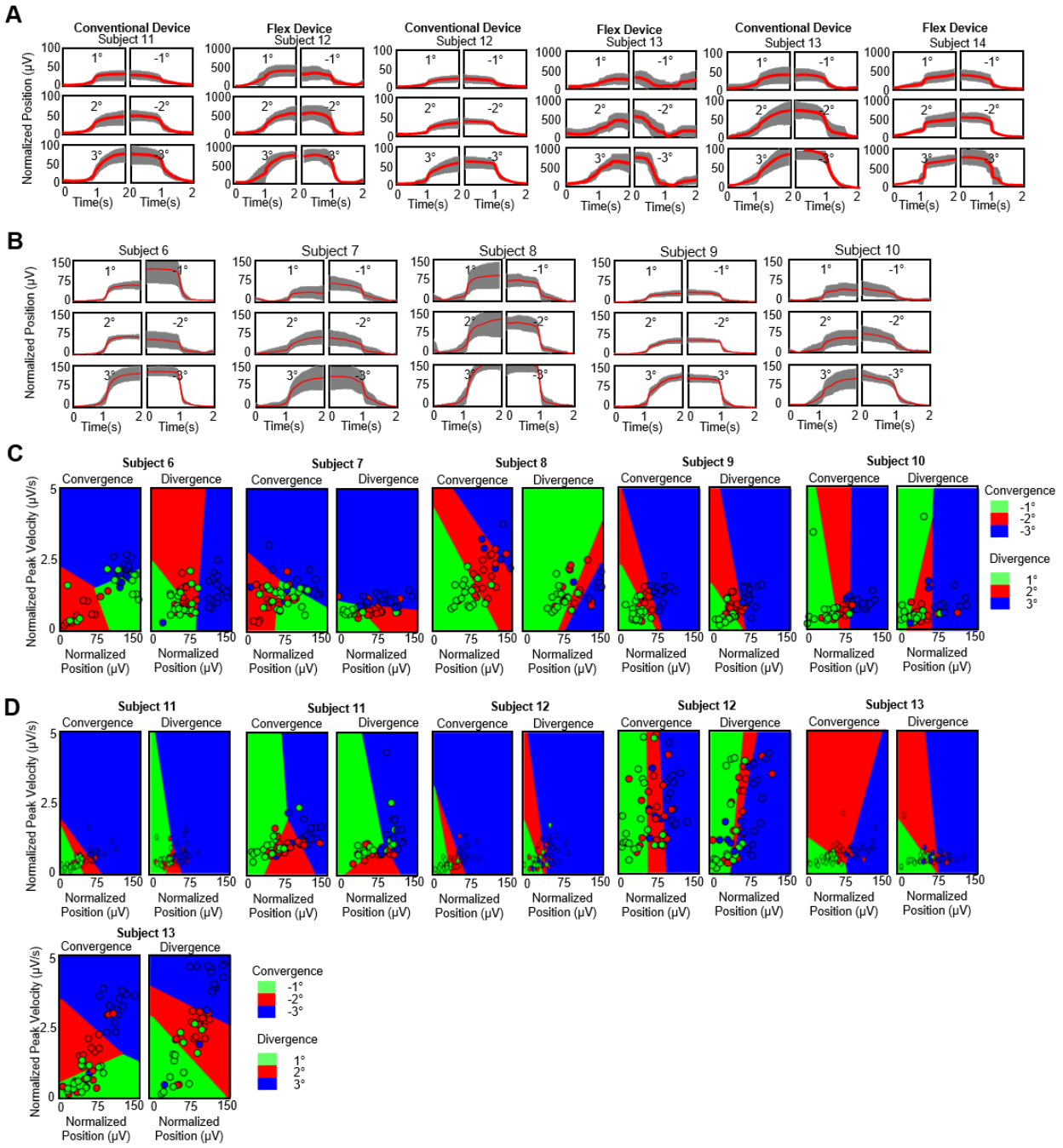

Figure S9. Performances of the periocular wearable electronics. (A) Normalized eye vergence motions recorded with subjects 11-13 using the virtual apparatus. The normalized signals for each user for all vergence motions indicate more precise responses in the VR display. (B) The normalized signals for each user from subjects 6-10 for all vergence motions indicate high variability with signal collection with physical apparatus. (C) Normalized peak velocity vs position for subjects 6-10 in physical apparatus. The virtual reality data from subjects 11-13 from eye therapy training program with decision boundaries. (D) The virtual reality data from subjects 11-13 from eye therapy training program with decision boundaries using the VR apparatus.

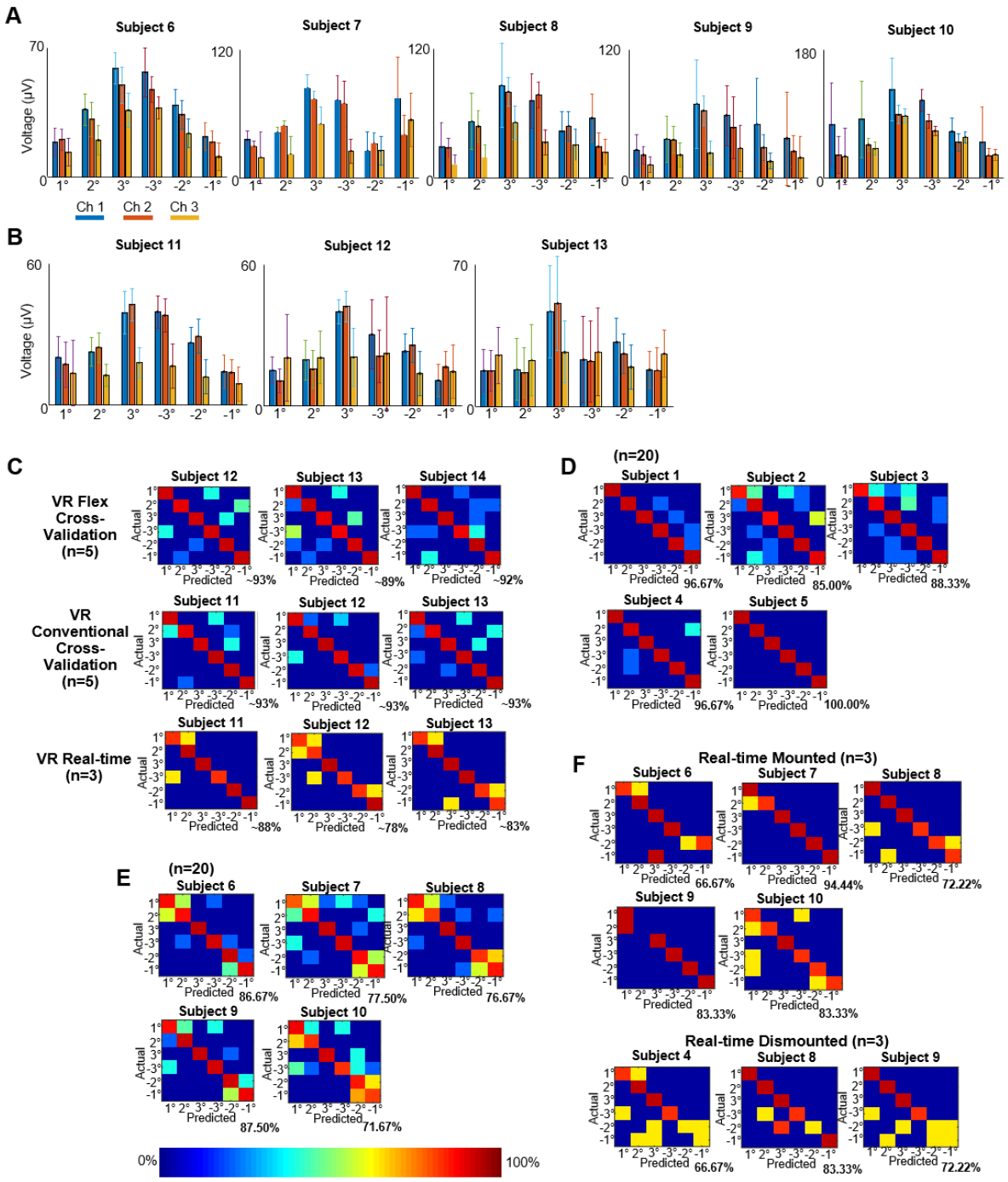

Figure S10. Performances of the periocular wearable electronics. (A-B) Average amplitudes for eye vergence training with physical apparatus showing the eye resolution using rise time method for physical apparatus from (A) subjects 6-10 and (B) subjects. (C) OV2 assessment of subjects 11-14 with cross-validation and real-time algorithm with corresponding real-time datasets. (D) OV2 cross-validation assessment of subjects 1-5 using the physical apparatus from eye vergence training with all 9 positions. Associated confusion matrix for the center position is shown. (E) OV1 cross-validation assessment of subjects 6-10 using the physical apparatus from eye vergence training with all 9 positions and the associated confusion matrix for the center position is shown. (F) Using OV1 and physical apparatus subjects 6-10 underwent eye vergence training with all 9 positions with the ocular mount, but only the center position is shown here. Real-time classification algorithm results under ocular mounting and dismounted conditions.

Supplementary Tables

Table S1. Feature comparison between BioRadio and periocular wearable electronics. Integration of advanced chip components allow the periocular wearable electronics to be equipped with comparable electronic performances to BioRadio while achieving the extremely light weight.

	BioRadio	**Periocular wearable electronics**
Wireless connection	Bluetooth Classic + LE	Bluetooth LE (4.2)
Data rate	190 kbps	120 kbps
Differential channels	4	Up to 8
Sampling resolution	Up to 24-bit	24-bit
Common mode rejection	-100 dB	-110 dB
Input impedance	500 MΩ	1000 MΩ
Capacity	8 GB	No Storage
Sample rate	250-16kHz	250-16kHz
Battery life	~9 hours (1320 mAh)	~1 hour (105 mAh)
Battery type	Lithium-ion polymer	Lithium-ion polymer
Device weight	115 g	5.5 g (3.3 g without battery)

Table S2. OV2 cross-validation accuracies of subjects 1-5 using the physical apparatus. Subjects 1-5 conducted eye vergence training with all 9 positions; the corresponding accuracies are shown here.

N = 20		All nine positions								
		Center	0°	45°	90°	135°	180°	215°	270°	315°
Percent of Accuracy of Each Subject	S1	96.67	96.67	95.00	98.33	97.50	99.17	96.67	97.50	95.83
	S2	85.00	82.50	85.83	83.33	88.33	90.83	93.33	89.17	89.17
	S3	88.33	91.67	95.00	94.17	95.00	93.33	91.67	92.50	88.33
	S4	96.67	87.50	95.00	96.67	98.33	90.00	89.17	93.33	95.00
	S5	100.00	90.83	95.83	91.67	95.83	95.00	100.00	95.00	93.33

Table S3. OV2 cross-validation accuracies of subjects 1-5 using the physical apparatus. Subjects 1-5 conducted eye vergence training with all 9 positions; the corresponding accuracies are shown here.

N = 20		All nine positions								
		Center	0°	45°	90°	135°	180°	215°	270°	315°
Percent of Accuracy of Each Subject	S1	96.67	96.67	95.00	98.33	97.50	99.17	96.67	97.50	95.83
	S2	85.00	82.50	85.83	83.33	88.33	90.83	93.33	89.17	89.17
	S3	88.33	91.67	95.00	94.17	95.00	93.33	91.67	92.50	88.33
	S4	96.67	87.50	95.00	96.67	98.33	90.00	89.17	93.33	95.00
	S5	100.00	90.83	95.83	91.67	95.83	95.00	100.00	95.00	93.33

Table S4. OV1 cross-validation assessment of subjects 6-10 using the physical apparatus. Subjects 6-10 conducted eye vergence training with all 9 positions; the corresponding accuracies are shown here.

N = 20		All nine positions								
		Center	0°	45°	90°	135°	180°	215°	270°	315°
Percent of Accuracy of Each Subject	S6	86.67	76.67	94.17	85.00	82.50	80.00	72.50	88.33	90.00
	S7	77.50	90.00	98.33	90.83	96.67	96.67	99.17	99.17	100.00
	S8	76.67	91.67	93.33	87.50	98.33	98.33	94.17	94.17	95.00
	S9	87.50	92.50	84.17	85.00	92.50	90.83	97.50	97.50	94.17
	S10	71.67	61.67	65.00	72.50	60.00	82.50	85.83	75.83	80.00

Table S5. OV2 real-time classification of test subjects using the physical apparatus. Subjects 6-10 underwent eye vergence training with all 9 positions with the ocular mount. Real-time classification algorithm results under mounted condition is presented.

N = 3		All nine positions								
		Center	0°	45°	90°	135°	180°	215°	270°	315°
Percent of Accuracy of Each Subject	S6	66.67	83.33	83.33	72.22	77.78	88.89	83.33	77.78	77.78
	S7	94.44	88.89	100.00	94.44	88.89	88.89	88.89	100.00	100.00
	S8	83.33	88.89	88.89	94.44	94.44	94.44	94.44	88.89	100.00
	S9	83.33	88.89	77.78	72.22	83.33	88.89	100.00	100.00	94.44
	S10	72.22	72.22	66.67	72.22	77.78	88.89	88.89	100.00	66.67

Table S6. OV2 real-time classification of test subjects using the physical apparatus. Subjects 4, 8 and 9 underwent eye vergence training with all 9 positions without the ocular mount. Real-time classification algorithm results under dismounted condition is presented.

N = 3		All nine positions								
		Center	0°	45°	90°	135°	180°	215°	270°	315°
Percent of Accuracy of Each Subject	S4	66.67	66.67	83.33	83.33	88.89	88.89	88.89	94.44	94.44
	S8	83.33	88.89	94.44	88.89	100.00	100.00	88.89	94.44	94.44
	S9	72.22	83.33	88.89	88.89	94.44	88.89	83.33	88.89	94.44

Supplementary Videos

Video S1. An example of a real-time vergence detection with a physical apparatus.

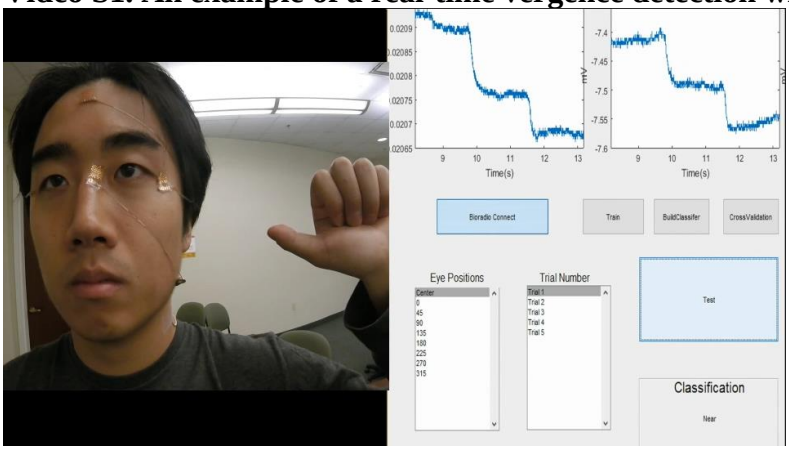

Video S2. An example of operation of a VR program – Brock string.

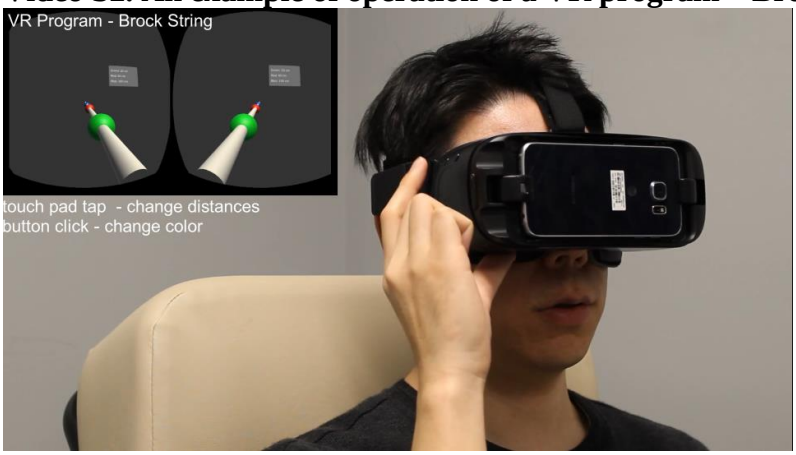

Video S3. An example of a real-time VR-based training apparatus.